MBoC | ARTICLE

Complex state transitions of the bacterial cell division protein FtsZ

Benjamin D. Knapp[a], Handuo Shi[b,c,*], and Kerwyn Casey Huang[a,b,c,d,*]
[a]Biophysics Program, Stanford University, Stanford, CA 94305; [b]Department of Microbiology and Immunology, Stanford University School of Medicine, Stanford, CA 94305; [c]Department of Bioengineering, Stanford University, Stanford, CA 94305; [d]Chan Zuckerberg Biohub, San Francisco, CA 94158

ABSTRACT **The key bacterial cell division protein FtsZ can adopt multiple conformations, and prevailing models suggest that transitions of FtsZ subunits from the closed to open state are necessary for filament formation and stability. Using all-atom molecular dynamics simulations, we analyzed state transitions of *Staphylococcus aureus* FtsZ as a monomer, dimer, and hexamer. We found that monomers can adopt intermediate states but preferentially adopt a closed state that is robust to forced reopening. Dimer subunits transitioned between open and closed states, and dimers with both subunits in the closed state remained highly stable, suggesting that open-state conformations are not necessary for filament formation. Mg^{2+} strongly stabilized the conformation of GTP-bound subunits and the dimer filament interface. Our hexamer simulations indicate that the plus end subunit preferentially closes and that other subunits can transition between states without affecting inter-subunit stability. We found that rather than being correlated with subunit opening, inter-subunit stability was strongly correlated with catalytic site interactions. By leveraging deep-learning models, we identified key intrasubunit interactions governing state transitions. Our findings suggest a greater range of possible monomer and filament states than previously considered and offer new insights into the nuanced interplay between subunit states and the critical role of nucleotide hydrolysis and Mg^{2+} in FtsZ filament dynamics.**

SIGNIFICANCE STATEMENT

- The cytoskeletal protein FtsZ forms filaments essential for bacterial cytokinesis. Traditional models focus on the transition of FtsZ subunits from closed to open states, but its importance for filament stability is unclear.
- Using molecular dynamics simulations, the authors discovered that *Staphylococcus aureus* FtsZ can exist in multiple stable states, with closed-state dimers exhibiting high stability, challenging previous notions about the necessity of open-state conformations for polymerization.
- This study broadens our understanding of FtsZ dynamics, suggesting a more complex interplay of states than previously thought. These insights could lead to novel approaches in developing antimicrobial strategies targeting bacterial cell division.

Monitoring Editor
Erin Goley
Johns Hopkins University

Received: Nov 22, 2023
Revised: Jul 25, 2024
Accepted: Jul 25, 2024

New Hypothesis

New Methods

INTRODUCTION

In eukaryotes and prokaryotes alike, cytoskeletal proteins play important roles in wide-ranging cellular processes that are intimately tied to the kinetics and mechanics of filament formation (Cabeen and Jacobs-Wagner, 2010; Fletcher and Mullins, 2010; Shaevitz and Gitai, 2010). The essential bacterial cell division protein FtsZ, a homologue of eukaryotic tubulin (Lowe and Amos, 1998), polymerizes into filaments that form a ring (the "Z-ring") at midcell that recruits other members of the division machinery (the "divisome") and guides the synthesis of new cell wall material (Bi and Lutkenhaus, 1991; Typas *et al.*, 2011). FtsZ filaments bind to the membrane through interacting partners ZipA and FtsA (Hale and de Boer, 1997; Conti *et al.*, 2018), and move along the division plane through treadmilling (Bisson-Filho *et al.*, 2017; Wagstaff *et al.*, 2017; Yang *et al.*, 2017). Filament formation and lateral association is thought to play an important role in organizing the divisome (Guan *et al.*, 2018). However, the range of possible states of FtsZ filaments has yet to be fully elucidated.

FtsZ is a GTPase, with the nucleotide-binding pocket located at its polymerization interface (Lowe and Amos, 1998, 1999). FtsZ polymerization is directly coupled to GTP hydrolysis, as intersubunit interactions are necessary for catalysis (Scheffers *et al.*, 2000; Oliva *et al.*, 2004; Ruiz *et al.*, 2022). Mg^{2+} is required for GTP hydrolysis and limits FtsZ depolymerization (Mukherjee and Lutkenhaus, 1999; Rivas *et al.*, 2000; Ruiz *et al.*, 2022). In many crystal structures of FtsZ filaments, subunits have been found to adopt an "open" state (often referred to as the "tense" or "T" state) in which the C-terminal domain (CTD) is farther from both the H7 helix and the N-terminal domain (NTD) than in the "closed" state (often referred to as the "relaxed" or "R" state) of monomer crystal structures (Fujita *et al.*, 2017; Wagstaff *et al.*, 2017). These structural studies have motivated the development of biophysical models relating FtsZ polymerization to conformational switching between the closed and open states (Wagstaff *et al.*, 2017), whereby the rare nature of opening events generates a nucleation barrier to polymerization and filament polarity emerges from the growing end (kinetic plus end) being locked into an open state (Corbin and Erickson, 2020). While most studies have focused on filament structures with subunits of *Staphylococcus aureus* and *Methanocaldococcus jannaschii* FtsZ in the open state (Wagstaff *et al.*, 2017; Oliva *et al.*, 2004), filaments of *Mycobacterium tuberculosis* FtsZ (Guan *et al.*, 2018), and of *Escherichia coli* FtsZ (Schumacher *et al.*, 2020; Yoshizawa *et al.*, 2020) have been crystallized with subunits in the closed state, although intersubunit interactions were weaker than for other FtsZ filament structures (Guan *et al.*, 2018; Schumacher *et al.*, 2020). In previous studies, *S. aureus* FtsZ (*Sa*FtsZ) mutants unable to form filaments were crystallized only as closed-state monomers (Wagstaff *et al.*, 2017), and mutations at filament interfaces produced weakly bound subunits in the closed state (Matsui *et al.*, 2014), suggesting that FtsZ monomers likely exist in the closed state and that the open state is important for polymerization. Additionally, *Sa*FtsZ filaments composed entirely of closed-state subunits were crystallized with weaker intrafilament interactions (Fujita *et al.*, 2017), further indicating the importance of open states in filament stability. Together, these studies suggest that transitions between closed and open states could play a major role in FtsZ filament assembly, but several major questions remain. In particular, the conditions under which monomers access open states and whether other states exist are unknown. Moreover, how subunits transition between states and whether factors such as divalent cations, nucleotide binding, and filament stability impact and/or are impacted by subunit states remain to be elucidated.

All-atom molecular dynamics (MD) simulations have proven a powerful tool for exploring the conformational dynamics and mechanics of cytoskeletal filaments, including FtsZ. Equilibrium MD simulations have revealed the presence of multiple twist states in double protofilaments of the bacterial actin homolog MreB (Shi *et al.*, 2020), and steered MD simulations demonstrated causal links between filament properties such as intrasubunit movements and filament bending (Colavin *et al.*, 2014). Microsecond-scale simulations of MreB double protofilaments revealed rapid transitions between twist states whose occupancy was dependent on the bound nucleotide, and deep learning algorithms proved effective for identifying intrasubunit interactions that are predictive of filament twist states (Knapp *et al.*, 2022). Due to its inherent dynamics and central importance to cell division, FtsZ in a variety of polymer structures has been a major focus of previous MD simulations. Equilibrium MD simulations successfully predicted that filament bending is sensitive to the bound nucleotide (Hsin *et al.*, 2012; Li *et al.*, 2013). Simulations of a G193D mutant in the H7 helix, a key structural feature involved in open-closed transitions (Wagstaff *et al.*, 2017), predicted that mutant filaments would adopt a twisted state, and indeed the mutant altered Z-ring structure from a ring to a helix in *S. aureus* cells (Pereira *et al.*, 2016). In simulations of *Sa*FtsZ heptamers, most subunits adopted an open state, similar to prevailing model predictions (Corbin and Erickson, 2020), although the kinetic plus end with a free CTD stabilized in a closed state (Ramirez-Aportela *et al.*, 2014). Simulations of *M. tuberculosis* FtsZ trimers suggested a link between filament stability and open-closed transitions (Lv *et al.*, 2021). However, these simulations have not systematically tested whether the open state is necessary for stable filament formation.

Here, we perform all-atom MD simulations of *Sa*FtsZ in monomer, dimer, and hexamer arrangements, and quantify how subunit state is affected by the bound nucleotide, the presence of Mg^{2+} in the nucleotide-binding pocket, and its initialized conformation. We discover states intermediate between closed and open and find that Mg^{2+} generally stabilizes the subunit state, regardless of filament arrangement. We find that dimers can persist with both subunits in the closed state without any loss of intersubunit stability. In a hexamer, the plus end rapidly closes, and the state of other subunits transitions along a continuum between closed and open but is stabilized by Mg^{2+} in the nucleotide binding pocket. A deep-learning algorithm successfully classified open and closed states regardless of the initial state of the filament, the bound nucleotide, or the presence/absence of Mg^{2+}. While current models of FtsZ polymerization and stability propose that open states are required for stable interaction and treadmilling, these findings suggest a more nuanced picture involving what is likely a complex set

This article was published online ahead of print in MBoC in Press (http://www.molbiolcell.org/cgi/doi/10.1091/mbc.E23-11-0446) on July 31, 2024.

*Address correspondence to: Handuo Shi (handuo@stanford.edu); Kerwyn Casey Huang (kchuang@stanford.edu).

Abbreviations used: bSASA, buried solvent accessible surface area; CTD, C-terminal domain; GDP, guanosine diphosphate; GTP, guanosine triphosphate; MD, molecular dynamics; *Mtb*FtsZ, *Mycobacterium tuberculosis* FtsZ; NTD, N-terminal domain; *Sa*FtsZ, *Staphylococcus aureus* FtsZ.

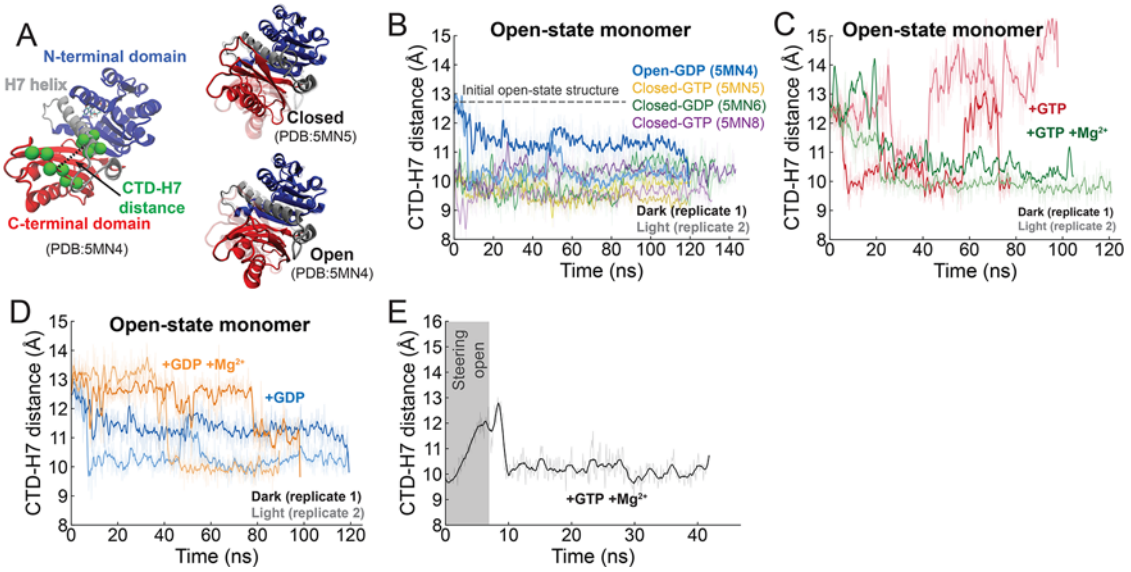

FIGURE 1: FtsZ monomers preferentially adopt a closed state that is stabilized by Mg^{2+}. (A) *Sa*FtsZ structures in the closed and open states. (Left) The CTD-H7 distance (dotted line, left) is defined as the distance between the centers of mass of two groups of residues (green spheres) from the CTD (red) and H7 helix (gray). (Right) The closed structure (top, 5MN5) is distinguished from the open state (bottom, 5MN4) by the hinging of the CTD toward the H7 helix. (B) Monomers typically adopt closed states. The open-closed metric (CTD-H7 distance) shows that GDP-bound monomers initialized in an open state rapidly close and that monomers with either bound nucleotide initialized in a closed-state remain closed (CTD-H7 distance ≈10 Å). (C) The transition of GTP-bound monomers initialized in an open state (PDB:5MN4, with the nucleotide replaced by GTP) to a closed state is stabilized by Mg^{2+}. (D) Mg^{2+} delays the closing of GDP-bound monomers initialized in an open state (PDB:5MN4). (E) The equilibrated closed state of a GTP-bound monomer with Mg^{2+} is highly stable. A GTP-bound monomer with Mg^{2+} equilibrated in a closed state (Figure 1C, light green) was steered with force sufficient to increase the CTD-H7 distance to >12 Å (shaded gray box). After reopening, the simulation of the system continued without steering force, and the monomer quickly reclosed. Each trajectory was smoothed using a moving Savitzky-Golay filter with a window of 2 ns and a 3rd-order polynomial, and raw trajectories are shown as thin, transparent lines. Replicates ($n = 2$) for each system are shown in light and dark shades.

of state transitions and additional mechanisms that determine FtsZ filament stability and polarity.

RESULTS

FtsZ monomers preferentially adopt a closed state that is stabilized by Mg^{2+}

Previous studies demonstrated that FtsZ monomers adopt a stable closed state (Ramirez-Aportela *et al.*, 2014; Wagstaff *et al.*, 2017) and that transitions between the open and closed states are likely coupled to polymerization dynamics (Fujita *et al.*, 2017; Wagstaff *et al.*, 2017; Ruiz *et al.*, 2022). Recently, nonpolymerizing mutants of *Staphylococcus aureus* FtsZ (*Sa*FtsZ) were crystallized and found locked in either open or closed forms (PDB: 5MN4[open, GDP-bound], 5MN5[closed, GTP-bound], 5MN6[closed, GDP-bound], 5MN8[closed, GTP-bound]; Wagstaff *et al.* 2017). The 5MN4 open-state structure was essentially identical to the previously solved wild-type GDP-bound filament structure (3VO8, α-carbon RMSD = 0.26 Å; Matsui *et al.*, 2012).

To assess the stability of open and closed monomers, we performed all-atom equilibrium MD simulations of the appropriate FtsZ structures, which were reverted to their wild-type amino acid sequences (*Materials and Methods*). Based on a previous MD study of FtsZ conformational states (Ramirez-Aportela *et al.*, 2014), we quantified the open/closed states using the distance between the centroids of two α-carbon clusters located on the CTD and the H7 helix (residues 196–202, 295–300; Figure 1A). Using this metric, open states are characterized by a distance of ∼13 Å (PDB: 5MN4) and closed states by a distance of 9–10 Å (PDB: 5MN5, 5MN6, 5MN8). Because open-closed transitions are largely determined by CTD movement (Wagstaff *et al.*, 2017), alternative open-closed metrics capturing CTD movement relative to the NTD have also been used; we found that the CTD-H7 distance was correlated with other metrics (CTD-NTD distance, $r = 0.76$; CTD-NTD angle, $r = 0.56$) across a broad range of simulation structures (Supplemental Figure S1, A and B), thus we assume that these metrics are approximately equivalent and utilize the CTD-H7 distance henceforth. FtsZ monomers initialized in the closed state remained in the closed state (9–10 Å) throughout each simulation ($n = 6$ replicates total across three crystal structures), independent of the nucleotide (Figure 1B). For a monomer initialized in the GDP-bound open state, one replicate quickly (<10 ns) closed to ∼10 Å, while the other replicate only partially closed to ∼11 Å and remained in this intermediate configuration for the rest of the 120-ns simulation (Figure 1B), which was significantly different from the closed state ($p < 0.001$). The RMSD relative to the initial crystal structure (*Materials and Methods*) was stable throughout all monomer simulations (2–3 Å), despite open-to-closed transitions (Supplemental Figure S1C). Note that the RMSD likely does not reflect open-closed state transitions because state transitions are dominated by local hinging of the CTD, while the RMSD is dominated by global residue reorganization during equilibration (as a reference, the RMSD between the 5MN4 and 5MN5 crystal structures is 3.1 Å, similar to the RMSD of an equilibrated monomer simulation from its crystal structure).

To evaluate how the bound nucleotide impacts open-to-closed transitions, we performed simulations initialized with the open-state monomer structure bound to GTP (*Materials and Methods*). Although both replicates closed within 30 ns, they later reopened, and then one replicate closed again by ~70 ns (Figure 1C), indicating that GTP-bound monomers can explore both states on short (tens of ns) time scales. To further explore these transitions, we considered the impact of Mg^{2+} on FtsZ conformational states (*Materials and Methods*). We found in MD simulations that Mg^{2+} delayed closing of GDP-bound open-state monomers by several tens of ns ($n = 2$ replicates, Figure 1D), while GTP monomers initialized in the open state with Mg^{2+} rapidly and stably closed (for >100 ns, $n = 2$ replicates; Figure 1C).

To examine the stability of the closed GTP-Mg^{2+} state at the end of the equilibrium simulation (Figure 1C), we performed steered MD simulations in which we attempted to reopen the closed monomer (*Materials and Methods*). Although a force constant of ~3.5 N/m was sufficient to reopen the GTP-Mg^{2+} monomer in ~10 ns, removing the force constraint resulted in very rapid (<2 ns) and stable closing (Figure 1E), suggesting that the closed state is highly favored. We further asked whether the open state could be stabilized via steering by initializing a GTP-Mg^{2+} monomer from the open crystal structure and constraining it in the open state for ~20 ns, similar to the duration over which GTP-bound monomers with Mg^{2+} stayed open in equilibrium simulations (Figure 1C). The monomer stayed open during steering but afterward slowly closed with some fluctuations, eventually reaching a closed state after ~90 ns (Supplemental Figure S1D). Thus, while steering the monomer open for an extended time could somewhat delay its access to the closed state, Mg^{2+} strongly stabilized GTP-bound monomers in the closed state.

During GTP hydrolysis, both the γ-phosphate group and Mg^{2+} exit the nucleotide-binding pocket, and GDP-bound monomers are spontaneously exchanged for GTP-Mg^{2+} (Ruiz *et al.*, 2022). Thus, GTP-Mg^{2+} and GDP monomers are likely the most physiologically relevant nucleotide states, which both stably closed when initialized from an open state.

Both open and closed states are accessible in stable FtsZ dimers

Prevailing models of FtsZ polymerization suggest that open-state conformations are required for intersubunit interactions within filaments owing to a favorable binding interface (Corbin and Erickson, 2020). If monomers predominantly exist in stable closed states, then dimer nucleation requires a transition from closed to open. A previous modeling study suggested that monomers exist in an equilibrium between open and closed states with an equilibrium constant of 5000–20,000 (closed:open; Corbin and Erickson, 2020), which would indicate that nucleation events are rare. Thus, we sought to evaluate the stability of dimers initialized in either open or closed conformations (*Materials and Methods*). We aligned *Sa*FtsZ monomer structures (PDB: 5MN4, 5MN5, 5MN6, and 5MN8; mutations reverted to wild type) to the structure of the *Sa*FtsZ straight filament (PDB: 3VO8; *Materials and Methods*) and performed MD simulations of dimers. Dimer stability was evaluated via the buried solvent-accessible surface area (bSASA) between the two subunits (*Materials and Methods*). All dimers initialized in the closed state initially exhibited a bSASA of ~800 Å^2, which rapidly decreased at the beginning of simulations by >400 Å^2 (Figure 2A), with some stabilizing at a bSASA significantly different from the open-state dimer ($p < 0.001$, two-sample *t*-test). Notably, some closed-state dimer replicates stabilized at very low bSASA (<300 Å^2), and one replicate completely dissociated (bSASA = 0 Å^2, Figure 2A). By contrast, GDP-bound dimers initialized from the open-state crystal structure exhibited a much higher initial bSASA (>1200 Å^2; Figure 2A). In both replicate simulations, bSASA initially decreased by ~300–400 Å^2, then slowly increased to ~1100 Å^2 (Figure 2A).

We found that GDP-bound dimer simulations initialized in the open state displayed diverse open-closed conformational transitions. In one replicate, the bottom subunit (CTD exposed, here referred to as P1; Figure 2B) rapidly and stably closed (Figure 2C, left), similar to the equivalent monomer (Figure 1B), while the top subunit (NTD exposed, P2; Figure 2B) remained open (Figure 2C, left). Similar dynamics, in which the P1 subunit closes, and the P2 subunit remains open, were observed in previous MD simulations of FtsZ filaments (Ramirez-Aportela *et al.*, 2014). Our other replicate simulation was characterized by continual changes in the P2 subunit's CTD-H7 distance between 10–13 Å, while the P1 subunit remained open for ~80 ns before rapid closure (Figure 2C, right).

Stable filaments have been previously described by the motif that the upper subunit (P2), whose CTD interacts with the NTD of the bottom subunit (P1; Figure 2B), remains open (Ramirez-Aportela *et al.*, 2014; Lv *et al.*, 2021). However, in simulations of a GDP-bound dimer initialized in the open state, we observed stable interactions between the subunits during intervals in which the P2 subunit was closed (Figure 2C, right). To assess whether closed subunits can assemble into stable filaments, we performed a refined interface-based alignment of closed-state GTP-bound monomers with the straight *Sa*FtsZ filament structure (*Materials and Methods*). Instead of aligning the whole monomer to the 3VO8 filament structure, we aligned the two closed-state monomers to the NTD of the bottom subunit and to the CTD of the top subunit, which represents the true filament interface between subunits (Ramirez-Aportela *et al.*, 2014; Fujita *et al.*, 2017; Wagstaff *et al.*, 2017; Du *et al.*, 2018). This alignment produced an initial bSASA near 1000 Å^2 (Figure 2D), higher than for the simple alignment procedure based on the 3VO8 structure (Figure 2A). In simulations of the interface-aligned dimer, bSASA slowly decreased to ~700 Å^2 (Figure 2D), while both subunits remained stably closed (Figure 2E). Based on our observation that the addition of Mg^{2+} increased the stability of the closed state for GTP-bound monomers (Figure 1C), we added Mg^{2+} to the interface-aligned GTP-bound closed dimer and found that the bSASA remained near its high initial value throughout the simulation, overlapping with the values characteristic of open-state GDP-bound dimers (Figure 2D). Furthermore, the subunits again remained closed throughout the simulations (Figure 2E), suggesting that stable interactions can occur even between closed FtsZ subunits.

To determine whether wild-type closed-state filaments in a native (unreverted) state are stable and whether subunits undergo open-closed transitions, we performed monomer and dimer simulations initialized from crystal structures of wild-type *Sa*FtsZ filaments solved in both open (PDB: 5H5G, chain A) and closed (PDB: 5H5G, chain B) states (Fujita *et al.*, 2017; Supplemental Figure S2). GDP-bound monomers exhibited the expected behaviors (Figure 1), with rapid closing of monomers initialized in the open state and closed-state monomers remaining closed (Supplemental Figure S2A). GDP-bound dimers initialized in the open state largely remained stable through the 100-ns simulation (bSASA >1000 Å^2), although the bSASA of one replicate decreased by 25% (Supplemental Figure S2B). Similar to our other open-state

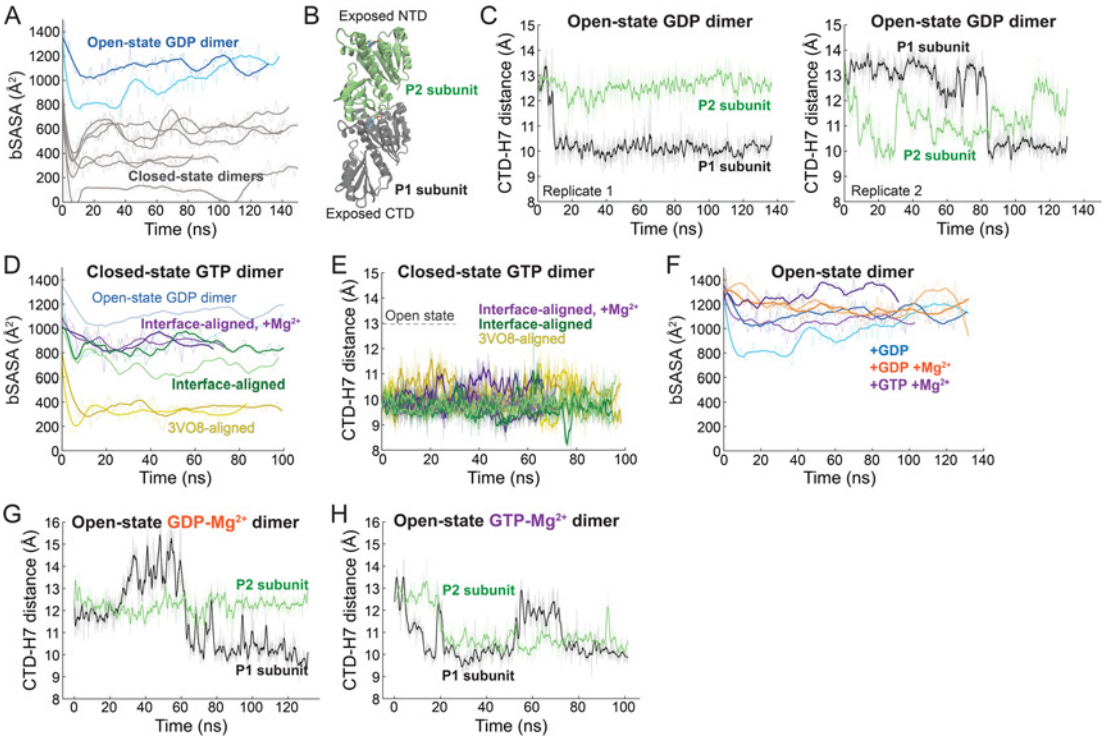

FIGURE 2: Subunits of stable dimers can adopt both open and closed states. (A) Using straight-filament alignments, FtsZ dimers are only stable when initiated from the open-state crystal structure, with stability characterized by high bSASA. Target crystal structures were aligned to the straight *Sa*FtsZ filament structure (3VO8) to generate dimers. The bSASA of open-state (PDB: 5MN4; blue) or closed-state (PDB: 5MN5, 5MN6, 5MN8; gray) dimers during equilibrium MD simulations is shown. Replicates ($n = 2$) for the open-state GDP-bound dimer are shown as light and dark shades, and replicates ($n = 6$ across three initial crystal structures) for closed-state dimers are colored gray. The significance between open and closed dimers was evaluated using a two-sample *t*-test for times > 40 ns ($p < 0.001$). (B) Dimer structure of *Sa*FtsZ in an open state (5MN4 aligned to 3VO8). The bottom subunit (P1, black) has an exposed CTD, and the top subunit (P2, green) has an exposed NTD and nucleotide. GDP is shown in each subunit's binding pocket. (C) Stable GDP-bound dimers initialized in the open state contain a mixture of open and closed subunits. (Left) The first replicate is characterized by stable closing of the P1 subunit while the P2 subunit remained stably open. (Right) The second replicate is characterized by rapid migration of the P2 subunit between open and closed states and delayed closing of P1. (D) Interface-aligned GTP-bound dimers initialized in the closed state are stabilized by Mg^{2+}. The refined interface alignment of 5MN5 (*Materials and Methods*) generated dimers with a higher initial bSASA (~950 Å^2, green) than simple subunit alignment (~800 Å^2, yellow). The addition of Mg^{2+} further stabilized the interface-aligned dimer (purple). The trajectory of the GDP-bound structure initialized in the open state (blue) is shown for comparison. Replicates ($n = 2$) for each system are shown as light and dark shades. (E) All subunits of a dimer initialized in the closed state remain stably closed. The CTD-H7 distances of all subunits in dimers constructed (simple alignment or interface-aligned) from the 5MN5 structure all remained at ~10 Å throughout equilibrium MD simulations. Replicates ($n = 2$) for each system are shown as light and dark shades, and subunits from each simulation have the same color. (F) Dimers with subunits initialized in the open state are stable with high bSASA, regardless of nucleotide or the presence of Mg^{2+}. Replicates ($n = 2$) for each system are shown as light and dark shades. (G) Addition of Mg^{2+} to GDP-bound dimers initialized in the open state enables exploration of higher CTD-H7 distances than are typical for the open state. The P1 subunit reached a CTD-H7 distance ~15 Å before eventually closing, while the P2 subunit remained stably open during equilibrium MD simulations. (H) Addition of Mg^{2+} to GTP-bound dimers initialized in the open state stabilizes the closed state in both subunits. The P1 and P2 subunits rapidly closed and remained at a CTD-H7 distance ~10 Å for most of the equilibrium MD simulation. Each trajectory was smoothed using a moving Savitzky-Golay filter with a window of 10 ns (A, C, D, and F) or 2 ns (E, G, and H) and a 3rd-order polynomial, and raw trajectories are shown as thin, transparent lines.

GDP-bound dimer simulations (Figure 2C), we observed multiple state transitions in each of the subunits, with one replicate stabilizing in an intermediate state with CTD-H7 distance ~11 Å (Supplemental Figure S2C). Both subunits of the wild-type GDP-bound dimers initialized in a closed state remained closed (Supplemental Figure S2D), and the bSASA was variable between replicates, decreasing by 20% in one replicate and increasing to overlap with one replicate of the open-state dimer in the other (Supplemental Figure S2B). These results provide further support that open-state dimers can explore multiple states while remaining stably bound, and that closed-state dimers can rearrange their interaction interface.

To further assess the impacts of Mg^{2+} on dimer behavior, we performed simulations of GDP- or GTP-bound dimers initialized in the open state with Mg^{2+} (Figure 2, F–H). GDP-bound dimers with Mg^{2+} remained highly stable (bSASA≈1200 Å^2; Figure 2F)

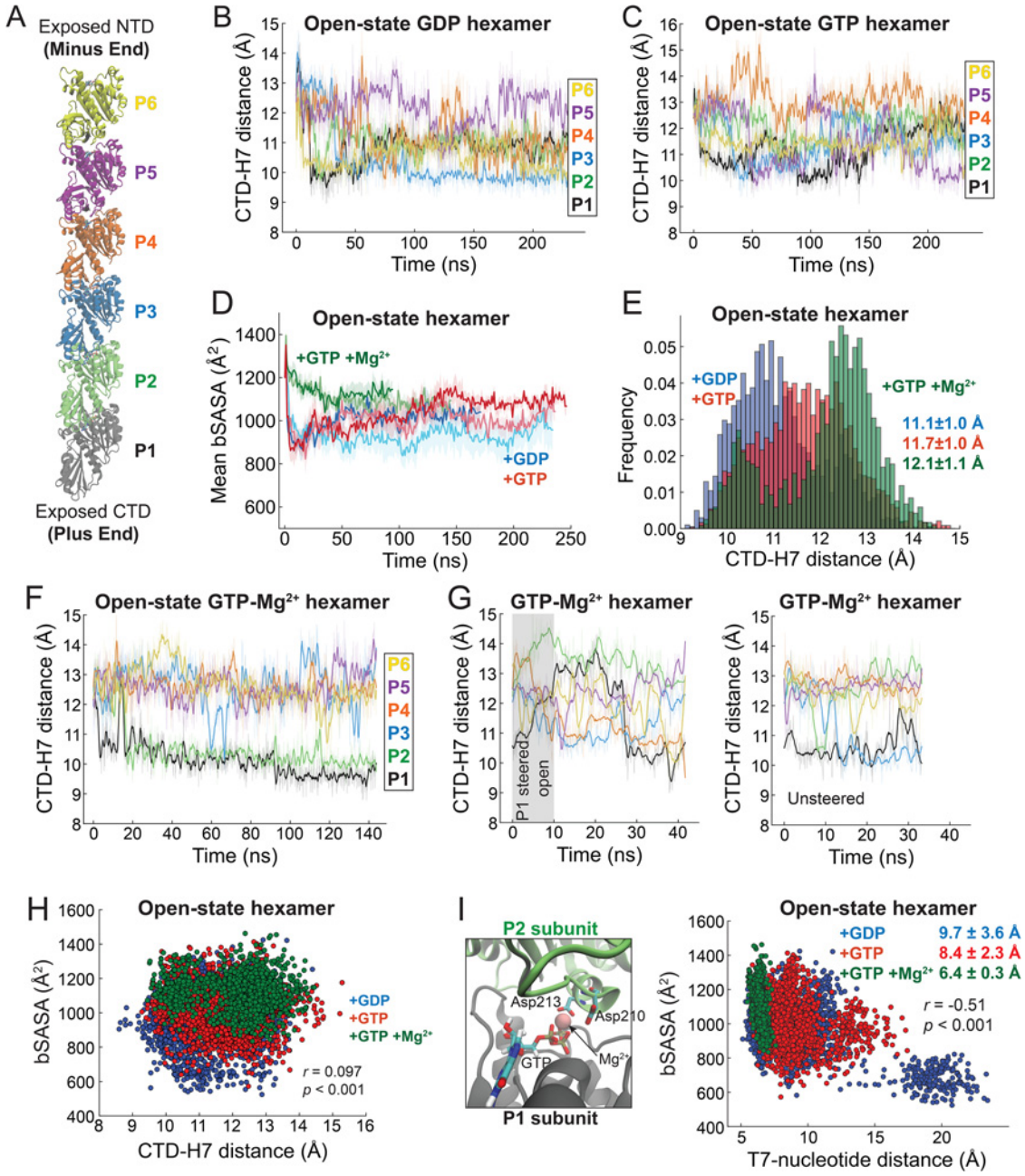

FIGURE 3: Intersubunit stability in hexamers is correlated with nucleotide-catalytic site interactions. (A) Hexamer *Sa*FtsZ structure (5MN4 aligned to 3VO8 straight filament) with subunits labeled P1 (kinetic plus end with exposed CTD) to P6 (kinetic minus end with exposed NTD). (B,C) GDP-bound (B) or GTP-bound (C) hexamer subunits initialized in the open state explore intermediate CTD-H7 distances. Shown are equilibrium MD trajectories of individual subunits labeled according to filament orientation in (A). (D) GTP-bound hexamers with subunits initialized in the open state are stabilized by Mg^{2+}. bSASA was computed across all five interfaces of the hexamer, and the mean is shown with shaded regions representing ± 1 standard error of the mean. Replicates ($n = 2$) are colored in dark or light shades. (E) The distribution of hexamer open and closed states is strongly affected by bound nucleotide and Mg^{2+}. Each histogram is an aggregate of all time points for both equilibrium MD simulation replicates, and numbers are the corresponding mean$\pm$1 SD. F) Mg^{2+} stabilizes open states in GTP-bound hexamers. Shown are equilibrium MD trajectories of individual subunits labeled according to filament orientation in (A). G) Reopening of the P1 subunit in a GTP-bound hexamer with Mg^{2+} causes conformational transitions in all other subunits. (Left) Steering open of the P1 subunit (black) from a CTD-H7 distance of ~10.5 Å to ~12.5 Å (shaded region). The initial structure was extracted from an early time point (6 ns) of the equilibrium MD simulation in (F). (Right) The unsteered control simulation exhibited a stably closed P1 subunit. H) Inter-subunit stability (bSASA) is not well correlated with CTD-H7 distance of the top subunit of the interface. Both replicates were aggregated, with Pearson $r = 0.097$ ($p < 0.001$). I) Intersubunit stability is negatively correlated with catalytic site interactions. (Left) The top subunit (green, P2) T7 loop with catalytic residues Asp210 and Asp213 (colored by element) are shown interacting with the coordinating Mg^{2+} (pink sphere) and GTP (colored by

and while the P2 subunit largely remained open in both replicates, the P1 subunit explored a wide range of CTD-H7 distances (Figure 2G; Supplemental Figure S3A). Similarly, GTP-bound dimers were stabilized by the addition of Mg^{2+} (Figure 2F), despite subunits stabilizing in either open, intermediate, or closed configurations (Figure 2H; Supplemental Figure S3B). These simulations suggest that Mg^{2+} stabilizes intersubunit interactions, which likely contributes to the impact of Mg^{2+} in FtsZ filament dynamics through the coordination of GTP hydrolysis (Mukherjee and Lutkenhaus, 1999; Rivas *et al.*, 2000; Ruiz *et al.*, 2022). These results indicate that neighboring subunits can remain tightly coupled both during subunit transitions between open and closed states and while the P2 subunit is closed.

FtsZ hexamer stability is determined by the bound nucleotide and Mg^{2+}

After GTP-bound monomers assemble into filaments, GTP hydrolysis destabilizes filaments (Ruiz *et al.*, 2022), providing a mechanism for filament-length homeostasis (Miraldi *et al.*, 2008; Corbin and Erickson, 2020). Previous MD simulations of FtsZ filaments demonstrated that GDP-bound filaments exhibited larger conformational fluctuations compared with GTP-bound filaments (Ramirez-Aportela *et al.*, 2014; Lv *et al.*, 2021), potentially indicating that GDP-bound filaments are less stable. Moreover, the stability of GTP-bound filaments is thought to be related to the preference of the subunits for the open state (Ramirez-Aportela *et al.*, 2014). However, because our dimer simulations displayed stable interfaces even between closed subunits, the precise determinants of intersubunit stability are likely a more complex interplay between open-closed transitions and nucleotide identity.

We sought to examine how inter-subunit interactions influence filament behavior via simulations of FtsZ hexamers (Figure 3A) bound to either GDP, GTP, or GTP and Mg^{2+}, enabling evaluation of intra-subunit dynamics across multiple interfaces and their coupling to large-scale stability. In simulations of GDP- or GTP-bound (without Mg^{2+}) hexamers, individual subunits underwent continual changes in CTD-H7 distance ranging between open and closed states (10–13 Å; Figure 3, B and C; Supplemental Figure S4, A and B), regardless of subunit location within the filament. Despite these conformational dynamics, the bSASA remained stable (Figure 3D), suggesting stable filament conformations. Mean CTD-H7 distance in GTP-bound filaments was somewhat higher than in GDP-bound filaments (11.1 ± 1.0 Å, 11.7 ± 1.0 Å; $p < 0.001$ two-sample *t*-test; Figure 3E), indicating that the open state is favored in GTP-bound filaments.

In the more physiologically relevant GTP-bound state with Mg^{2+} (Ruiz *et al.*, 2022), the initial structure was stabilized, maintaining a high bSASA throughout the entire simulation, in contrast to the initial drop in bSASA observed in GDP- and GTP-bound hexamers without Mg^{2+} (Figure 3D). Furthermore, while transitions occasionally occurred between open and closed states in GTP-bound hexamers with Mg^{2+}, the CTD-H7 distance largely stabilized at either 10 or 13 Å (Figure 3, E and F; Supplemental Figure S4C), with one replicate exhibiting stable closure of the P1 and P2 subunits (Figure 3F). Overall, GTP-bound hexamers with Mg^{2+} exhibited a bimodal distribution of CTD-H7 distance with a slightly higher mean (12.1 ± 1.1 Å) than hexamers without Mg^{2+} (Figure 3E), reflecting the tendency of subunits to remain open.

Previous *in vitro* and *in silico* studies demonstrated that FtsZ filament mechanics are nucleotide dependent, with GTP hydrolysis inducing an unstable GDP-bound interface and hence a softer filament (Lu *et al.*, 2000; Hsin *et al.*, 2012; Ramirez-Aportela *et al.*, 2014). To evaluate the mechanical properties of our hexamer simulations, we calculated the persistence length (L_p, *Materials and Methods*) and found that GDP-bound filaments were indeed softer ($L_p = 151 \pm 36$ nm) than GTP-bound hexamers without ($L_p = 469 \pm 77$ nm) and with Mg^{2+} ($L_p = 286 \pm 27$ nm) (Supplemental Figure S4F). These results were ∼2.5-fold lower than the reported value of 1150 nm for GTP-bound *Ec*FtsZ filaments formed at 20°C as measured using cryogenic electron microscopy (Turner *et al.*, 2012), which may be due to both species-specific properties (*Sa*FtsZ vs. *Ec*FtsZ) and filament softening at the higher temperature (37°C) in our simulations (Geggier *et al.*, 2011).

Open/closed conformations do not determine intersubunit stability

FtsZ filaments have the opposite kinetic polarity of tubulin, wherein the exposed CTD on the P1 subunit is the site of additional subunit binding (the plus end; Du *et al.*, 2018; Figure 3A). As such, previous studies have focused on the P1 subunit, which is typically assumed to be locked into the open state in a polymer, providing a favorable binding interface (Fujita *et al.*, 2017; Wagstaff *et al.*, 2017; Corbin and Erickson, 2020). However, in each of our multisubunit simulations, the P1 subunit was most likely to adopt and remain in a closed state (Figures 2 and 3; Supplemental Figure S3 and S4), similar to previous MD simulations of *Sa*FtsZ filaments (Ramirez-Aportela *et al.*, 2014). (Note that the subunit with a free CTD was referred to as the minus end in [Ramirez-Aportela *et al.*, 2014], a view that has now been revised [Du *et al.* 2018]). To probe the stability of the closed P1 subunit in hexamers, we performed steered MD simulations to reopen P1 in a preequilibrated GTP-Mg^{2+} hexamer (Figure 3G; *Materials and Methods*). Steering P1 open caused a slight increase in the CTD-H7 distance in the already open P2 subunit, while inducing closure of all other subunits (Figure 3G, left). Release of the steering force was accompanied by rapid dynamics of all subunits, and P1 reclosed within 20 ns (Figure 3G, left). In contrast, the unsteered filament continued with largely stable open/closed states (Figure 3G, right). Importantly, rapid subunit conformational dynamics during steering were not accompanied by loss of intersubunit stability (Supplemental Figure S4D). These results suggest that the P1 subunit highly favors the closed state, and its reopening induces filament-wide subunit closure without loss of stability.

Previous FtsZ studies suggested that occupation of the open state is correlated with intersubunit stability (Ramirez-Aportela *et al.*, 2014; Matsui *et al.*, 2014; Fujita *et al.*, 2017; Wagstaff *et al.*, 2017; Schumacher *et al.*, 2020; Yoshizawa *et al.*, 2020; Ruiz *et al.*, 2022), because the open state presents an exposed CTD favorable

element) of the nucleotide binding pocket of the bottom subunit (black, P1). T7-nucleotide distance reflects the distance between the catalytic residues (Asp210, Asp213) and the terminal (gamma) phosphate group of the bound nucleotide (GTP was aligned to GDP to account for virtual shift) (*Materials and Methods*). (Right) bSASA was negatively correlated with T7-nucleotide distance across all hexamer simulations (aggregated by replicates). Mean T7-nucleotide distances are reported for each system ±1 SD. The aggregate Pearson $r = -0.55$ ($p < 0.001$). Each trajectory was smoothed using a moving Savitzky-Golay filter with a window of 2 ns (B, C, F–H) or 10 ns (D) and third-order polynomial, and raw trajectories are shown as thin, transparent lines.

for binding (Matsui *et al.* 2014; Ruiz *et al.*, 2022). One MD study of straight *Mtb*FtsZ trimer filaments reported a positive correlation between bSASA and the CTD-NTD distance of the top subunit in some individual simulations (Lv *et al.*, 2021), but this correlation did not hold over all simulations collectively (Supplemental Figure S4E). In our simulations, bSASA was only very weakly correlated with CTD-H7 distance across hexamer simulations, either individually ($-0.11 < r < 0.094$, Supplemental Figure S4G) or collectively ($r = 0.097$, Figure 3H). Together, these results suggest that open-closed conformational switches alone do not affect intersubunit stability.

Intersubunit stability depends on catalytic site interactions

Filament assembly is required for GTP hydrolysis in FtsZ, as catalytic residues on the flexible T7 loop in the CTD of one subunit must engage with GTP in the nucleotide-binding pocket in the NTD of the adjacent subunit (Matsui *et al.*, 2014). Hydrolysis is important for driving filament dynamics and associated treadmilling (Du *et al.*, 2018; Wagstaff *et al.*, 2017; Ruiz *et al.*, 2022). Previous structural and biochemical work showed that interactions between the catalytic T7 loop and GTP are important for stabilizing open states and are critical to intersubunit stability (Matsui *et al.*, 2014).

In our simulations, we found that the distance between the main catalytic residues from the T7 loop (Asp210, Asp213 in *Sa*FtsZ; Matsui *et al.*, 2014) and the terminal phosphate group of the nucleotide (hereafter referred to as the T7-nucleotide distance, *Materials and Methods*) exhibited a negative correlation with bSASA ($r = -0.51$, $p < 0.001$; Figure 3I). Importantly, the coordinated Mg^{2+} stabilizes the interaction between the catalytic residues and the γ-phosphate of GTP (Figure 3I, left; Matsui *et al.*, 2014; Ruiz *et al.*, 2022), contributing substantially to subunit interface stability (Ramirez-Aportela *et al.*, 2014). Consistent with our observation above that the conformation of the top subunit (with exposed CTD) was not correlated with intersubunit stability (Figure 3H), the T7-nucleotide distance was only weakly correlated with the CTD-H7 distance ($r = -0.15$; Supplemental Figure S4H). These findings suggest that nucleotide interactions are a greater determinant of intersubunit stability than subunit open/closed conformation.

A deep-learning model predicts intrafilament open and closed states based on monomer trajectories

Recently, deep-learning approaches have become powerful tools for protein structure prediction (Jumper *et al.*, 2021; Bordin *et al.*, 2023), including the prediction of structural variants that may contribute to human disease (Blaabjerg *et al.*, 2023; Chandra *et al.*, 2023). DiffNets, a set of self-supervised autoencoders, was used to identify structural determinants across variants in beta-lactamase MD simulations (Ward *et al.*, 2021). Furthermore, these models were extended to predict key residues in double protofilament twist dynamics of the bacterial actin homolog MreB (Knapp *et al.*, 2022), connecting large-scale dynamics in protein complexes to subtle atomistic determinants.

To learn key intrasubunit interactions that determine open and closed states, we trained a DiffNet on open/closed states. Training data were extracted from a subset of monomer trajectories of *Sa*FtsZ bound to GDP without or with Mg^{2+}, structures that explored both open and closed states (Figure 1D). DiffNets was able to clearly distinguish open from closed states within these training data (Figure 4A), and DiffNets scoring of all trajectories of GDP-bound monomers without and with Mg^{2+} was highly correlated with CTD-H7 distance, even though the states with intermediate distance were not included in the training data ($r = 0.91$, Figure 4B). Thus, DiffNet training captured open-closed transitions that traverse intermediate states.

Analysis of key residues (defined as those present in >5 of the top 50 residue-residue interactions) identified G193 and E274 as highly important for determining the open/closed state (Figure 4C). Interestingly, mutations at G193 in *S. aureus* confer resistance to the antibiotic PC190723 (Haydon *et al.*, 2008), a drug that is thought to target the conformational switch between open and closed states (Matsui *et al.*, 2012; Ramirez-Aportela *et al.*, 2014). Furthermore, the top five residue-residue interaction pairs all involved the CTD, and either the H7 helix or the NTD (Supplemental Figure S5A), consistent with the CTD-H7 metric (Figure 1A) and suggesting that CTD movement dominates conformational switches (Ramirez-Aportela *et al.*, 2014; Wagstaff *et al.*, 2017).

DiffNets scoring of trajectories of GTP-bound monomers with or without Mg^{2+} was also highly correlated with CTD-H7 distance ($r = 0.79$, Supplemental Figure S5B), even though all training data involved GDP-bound monomers. Scoring of the subunits in GDP-bound dimers was similarly highly correlated with CTD-H7 distance ($r = 0.93$ and 0.82 for two replicates, Supplemental Figure S5C), as was scoring of GDP-bound hexamer subunits ($r = 0.70$ and 0.58 for two replicates, Figure 4D; Supplemental Figure S5D) and GTP-bound hexamer subunits with Mg^{2+} in one replicate simulation ($r = 0.82$, Figure 4E).

Interestingly, in the other replicate simulation of a GTP-bound hexamer with Mg^{2+}, DiffNets scores were highly correlated with CTD-H7 distance for all subunits except P4 (Supplemental Figure S5E), which exhibited high CTD-H7 distance characteristic of the open state but transitioned from high to low DiffNets score between $t = 30$–40 ns (Supplemental Figure S5F). As a result, the correlation coefficient was reduced from 0.76 (without P4) to 0.45 (considering all subunits). To determine whether the P4 subunit was in a distinct conformation from the rest of the subunits with high CTD-H7 distance, we also computed the CTD-NTD distance (Lv *et al.*, 2021). Although the two distances were generally highly correlated (Supplemental Figure S1A), the CTD-NTD distance of the P4 subunit exhibited a transition from 30 Å (open) to 26 Å (closed) between $t = 30$–40 ns (Supplemental Figure S5F), to a final value below that of any of the other subunits, consistent with its very low DiffNets scores during this interval. DiffNets scores were highly correlated with CTD-NTD distance for the P4 subunit alone ($r = 0.96$) and all subunits collectively ($r = 0.83$, Supplemental Figure S5G), and similarly for the simulations of GDP-bound hexamers ($r = 0.88$ and 0.74 for the two replicates in Figure 4D; Supplemental Figure S5D, respectively). These findings indicate that the CTD-H7 and CTD-NTD distances can be uncoupled in certain situations and that DiffNets scores for some systems can be more representative of states defined by CTD-NTD distance despite training based on states defined by CTD-H7 distance.

These results indicate that intra-filament subunit open-closed transitions are largely consistent with monomer conformations, despite the presence of inter-subunit interactions. In addition, the ability of the DiffNet trained on GDP-bound monomers (Figure 4, A and B) to predict open/closed states of GTP-bound subunits (Figure 4E; Supplemental Figure S5, B, E–G) suggests that open/closed conformations are not solely limited by nucleotide identity.

DISCUSSION

Our simulations show that FtsZ subunits may be able to adopt both open and closed states in any filament arrangement (Figures 2 and

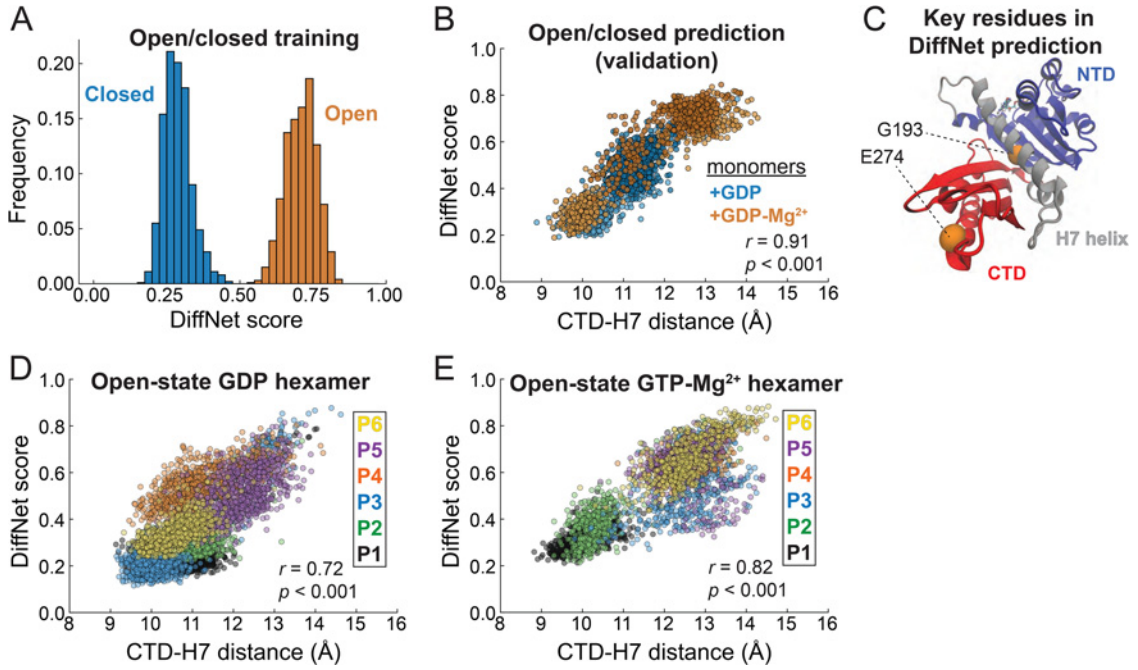

FIGURE 4: DiffNet predicts a continuous conformational landscape involving key residue-residue interactions that impact division *in vivo*. A) DiffNet training results in nonoverlapping score distributions for open and closed FtsZ monomer states. Open-state structures were extracted from simulations of GDP-bound monomers with Mg^{2+} (Figure 1D) and closed-state structures were extracted from a simulation of a GDP-bound monomer without Mg^{2+} (Figure 1D; *Materials and Methods*). B) DiffNet scoring on validation data is in excellent agreement with CTD-H7 distance. Shown are simulation trajectories from Figure 1D, with replicates ($n = 2$) in light and dark shades. The aggregate Pearson $r = 0.91$ ($p < 0.001$). C) DiffNet training identified two key residues at G193 and E274 (orange spheres). Key residues are defined as present in >5 of the top 50 residue-residue interactions used in the trained DiffNet classification. D) DiffNet scoring of GDP-bound hexamer subunits is in good agreement with CTD-H7 distance. Shown are data from trajectories of each subunit P1–P6 (labeled according to orientation from Figure 3A) for a single replicate simulation (Figure 3B). The aggregate Pearson $r = 0.72$ ($p < 0.001$). E) DiffNet scoring of GTP-bound hexamer subunits with Mg^{2+} is in good agreement with CTD-H7 distance. Shown are data from trajectories of each subunit P1–P6 (labeled according to orientation from Figure 3A) for a single replicate simulation (Figure 3F). The aggregate Pearson $r = 0.82$ ($p < 0.001$).

3). Crystal structures of *Sa*FtsZ have been solved with subunits exclusively in either the open or closed conformation (mostly open), and the subunits in a recent structure of a *Klebsiella pneumoniae* filament were exclusively in the open conformation (Fujita *et al.*, 2023). These results are likely due to the open state representing the most favorable binding state during crystallization, whereas MD simulations provide a sampling of available states that are thermodynamically inaccessible to crystallization conditions. Moreover, there is likely a broad range of possible subunit states, as evidenced by the stable intermediate observed in both monomer (Figure 1B) and hexamer (Figure 3, B and C; Supplemental Figure S4, A and B) simulations and by the correlation of DiffNets scores with CTD-H7 distance across the entire range of distances (9–15 Å; Figure 4, D and E; Supplemental Figure S5). In future studies, it will be interesting to investigate whether the binding of other divisome proteins such as ZipA and FtsA (Hale and de Boer, 1997; Conti *et al.*, 2018), membrane binding (Ramirez-Diaz *et al.*, 2021), or lateral association between FtsZ filaments (Guan *et al.*, 2018) impact subunit state occupancy.

In agreement with previous studies, we found that *Sa*FtsZ monomers preferentially adopt a closed state (Figure 1; Wagstaff *et al.*, 2017), filament formation causes the majority of subunits to stably adopt an open state (Figures 2 and 3; Matsui *et al.*, 2014; Fujita *et al.*, 2017; Wagstaff *et al.*, 2017) particularly in the presence of Mg^{2+} (Figure 3; Ramirez-Aportela *et al.*, 2014; Ruiz *et al.*, 2022), and GTP-bound hexamers are more rigid and stable than GDP-bound hexamers (Figure 3; Ramirez-Aportela *et al.*, 2014; Lu *et al.*, 2000). However, in contrast to previous studies, we found that monomers can adopt intermediate states (Figure 1, B and D) and that transiently maintaining an already open monomer in the open state through steering delays closing (Supplemental Figure S1D). Moreover, by aligning the interacting CTD/NTD of neighboring subunits (interface alignment, *Materials and Methods*), we constructed a dimer that persisted with both subunits in the closed state without loss of intersubunit stability (Figure 2, D and E), and simulations of more native-like closed dimers similarly produced stable dimers with a weaker intrafilament interface (Supplemental Figure S3). Additionally, the stability of hexamer subunit state was highly dependent on the presence of Mg^{2+} (Figure 3; Supplemental Figure S4), which has been left out of many previous MD simulations of FtsZ. Perhaps most importantly, intersubunit stability was largely uncorrelated with open-closed transitions (Figure 3H; Supplemental Figure S4, E and F), arguing against models in which filament subunits must adopt the open state to form a stable filament. Rather, we found that inter-subunit stability was negatively correlated with T7-nucleotide distance (Figure 3I), a measure of the distance between the catalytic residues on FtsZ's T7 loop and the terminal phosphate of the neighboring

subunit, suggesting a role for catalytic interactions in stabilizing filaments.

As in our previous study of the twist states of MreB (Knapp *et al.*, 2022), the deep learning framework DiffNets provided insight into intrasubunit interactions important for classifying subunit state (Figure 4; Supplemental Figure S5). Many of these interactions involved G193 (Figure 4C), a residue previously identified as highly impactful on FtsZ filament ultrastructure *in vivo* (Pereira *et al.*, 2016). Even though we trained the DiffNet model on states defined by the CTD-H7 distance (Figure 4A; *Materials and Methods*), DiffNets scores in some simulations were more highly correlated with CTD-NTD distance (Supplemental Figure S5, F and G), whose trajectory occasionally differed qualitatively from CTD-H7 distance. Thus, the DiffNet learned distinct features of both metrics. The cases in which these two metrics are separable suggest that other "closed" FtsZ conformations could exist that have a high CTD-H7 distance. Future studies should investigate whether a multidimensional metric can capture and predict state transitions with even more efficacy than we achieved here.

Current models for treadmilling postulate that, based on crystallization of open-state filaments, the plus-end subunit is locked in an open state to promote a favorable and polarized binding site (Wagstaff *et al.*, 2017; Corbin and Erickson, 2020), but our simulations and a previous study (Ramirez-Aportela *et al.*, 2014) suggest that the plus end subunit is actually more likely to adopt the closed, monomer conformation (Figure 3; Supplemental Figure S4). Additionally, our results suggest that many conformational subunit states are accessible within stable filaments (Figure 3), and nucleotide interactions within the binding pocket may play a larger role in inter-subunit stability than conformational switches alone (Figure 3, D, E, H, and I). How polarization is maintained across the filament to ensure that the plus end is favorable for subunit addition (and therefore promote treadmilling) is unclear from our results. Future polymerization models of FtsZ may require consideration of a multitude of conformational states and the particular importance of nucleotide exchange (Ruiz *et al.*, 2022), as well as the introduction of asymmetry and polarity by membrane binding and FtsZ cofactors (e.g., FtsA; Loose and Mitchison, 2014), to clarify the mechanism of treadmilling. Furthermore, how filament nucleation occurs from two stable, closed-state monomers is unclear – evidence suggests that dimer nucleation is cooperative (Chen *et al.*, 2005; Huecas *et al.*, 2008), as GTP-Mg^{2+} monomers must transition from a closed (monomer) to open state (filament; Ruiz *et al.*, 2022). In combination with our results, previous proposals (Ramirez-Aportela *et al.*, 2014) that the barrier to closed–closed dimer nucleation may be lower than assumed in most models (Corbin and Erickson, 2020) likely necessitate consideration of dimer–dimer interactions as a larger contributor to filament assembly than previously considered.

FtsZ filament conformation must adjust to reorganize the Z-ring during cell constriction. Ultimately, FtsZ filament conformation may affect cell division through nucleotide hydrolysis, (de-)polymerization, and treadmilling, about which our simulations have provided some new insights. The multiple states that we identified across filament arrangements may have differential occupancy across bacterial species, as has been suggested by the differential resistance of species to the inhibitor PC190723 (Miguel *et al.*, 2015), which binds to the CTD-H7 cleft and locks subunits into an open state (Andreu *et al.*, 2010; Matsui *et al.*, 2012). The existence of many FtsZ crystal structures, including the *E. coli* filament of closed subunits (Schumacher *et al.*, 2020; Yoshizawa *et al.*, 2020), should provide a springboard for comparative studies across bacteria that sheds light on the mechanistic links between FtsZ structure and function.

MATERIALS AND METHODS

Simulated systems

MD simulations performed in this study are described in Supplemental Table S1. All systems were prepared using VMD v. 1.9.3. The bound nucleotide was replaced by GTP or GDP for all simulated systems, a bounding water box with 17 Å padding was added to surround the complex, and sodium or chloride ions were added to neutralize the simulated system with the VMD plugin *autoionize* (establishing a zero net charge of the system). Crystal structures with mutant residues (PDB: 5MN4, 5MN5, 5MN6, 5MN8) were reverted to their wild-type amino acids with the VMD *mutate* and *guesscoord* commands. Mg^{2+} was added to select FtsZ structures via alignment with the *Methanocaldococcus jannaschii* FtsZ structure 1W5A (Oliva *et al.*, 2004). Filaments (dimers, hexamers) were constructed by aligning crystal structures to the FtsZ straight filament structure 3VO8 using the *mono2poly* VMD script, except for the interface-aligned closed-state dimers, which were aligned based on the interacting CTD and NTD of 3VO8 as detailed below.

Closed-state interface alignment

Closed-state dimers were stabilized beyond initial 3VO8 alignment by first aligning the 5MN5 (wild-type reverted) closed structure's NTD (residues 13–200) to the P1 subunit's NTD from a 3VO8 dimer. Then, the 5MN5 (wild-type reverted) closed structure's CTD (residues 225–315) was aligned to the P2 subunit's CTD from the 3VO8 dimer. This strategy generated an interface-aligned closed-state structure with a bSASA of 950 $Å^2$.

Equilibrium MD simulations

Simulations were set up as previously described (Shi *et al.*, 2020). Briefly, the CHARMM36 force field (Best *et al.*, 2012) and CMAP corrections (Mackerell *et al.*, 2004) were used, with water molecules described with the TIP3P model (Jorgensen *et al.*, 1983). The integration time step was 2 fs (Tuckerman *et al.*, 1992). Bonded terms and short-range, nonbonded terms were evaluated every time step, and long-range electrostatics were evaluated every other time step. The temperature was set to 310 K, and energy minimization was performed for the first 5000 timesteps. Setup, analysis, and rendering of the simulation systems were performed with VMD (Humphrey *et al.*, 1996). All analysis was performed on 0.1 ns frame intervals, except for bSASA calculations (1.0 ns frame interval). Python 3.6 was used for all subsequent analyses.

Most simulations were performed on the Expanse CPU cluster (San Diego Supercomputer Center) using NAMD 2.14 (Supplemental Table S1). Additional simulations were performed on a custom-built workstation ("Nova", Supplemental Table S1) with an NVIDIA RTX 4090 GPU, Intel i9-13900K CPU, and 64GB DDR5 RAM, using NAMD 3.0 with GPU acceleration.

CTD-H7 distance calculations

Following a previously proposed metric (Ramirez-Aportela *et al.*, 2014) for defining open and closed states, the CTD-H7 distance was measured as the distance between the centroids of the α-carbons of residue groups 196–202 (located within the H7 helix) and 295–300 (located within the CTD).

Steered MD simulations

Steered simulations were performed with the collective variables (*colvars*) constraint in NAMD, in which a harmonic restraint with

force constant 5.0 kcal/mol/Å^2 was used to steer α-carbons of residue groups 196–202 and 295–300 (which define the CTD-H7 distance) to a CTD-H7 distance of 13.3 Å. For the GTP-bound monomer with Mg^{2+}, steering was applied to either an equilibrated monomer (Figure 1C) or the initial open-state structure. Steering of the P1 subunit within the GTP-bound hexamer with Mg^{2+} was performed based on the hexamer filament structure after an initial six ns of equilibration simulation, during which only P1 closed (Figure 3F), and then applying the same restraint on the P1 subunit as on monomers.

Calculation of bSASA

The buried SASA between two molecules was calculated from three quantities: the SASA of each molecule by itself (denoted as A_1 and A_2), and the SASA of the complex of the two molecules when interacting (denoted as A_{1+2}). The bSASA between the two molecules is

$$\text{bSASA} = \frac{A_1 + A_2 - A_{1+2}}{2}.$$

For each molecule or molecule complex, its corresponding SASA was calculated in VMD using the command *measure sasa*, with 1.40 Å as the van der Waals radius for water molecules.

Calculation of filament persistence length

The persistence length (L_p) of FtsZ filaments was calculated by measuring the correlation function of inter-subunit vectors (d_i, d_{i+k}), which was modeled according to (Gittes *et al.*, 1993):

$$\langle d_i \cdot d_{i+k} \rangle = \langle \cos\theta_{i,i+k} \rangle = e^{-\frac{\Delta x}{L_p}}.$$

Here, d_i represents the vector between the centers of mass of the i and $i+1$ subunits and Δx is the distance between the i and $i+k$ subunits. Linear fitting was performed on Δx versus $-\ln\langle\cos\theta_{i,i+k}\rangle$ to extract the slope, L_p.

T7-nucleotide distance

The distance between the catalytic residues and the nucleotide's terminal phosphate was defined as the *T7-nucleotide distance*. This distance was computed by first measuring the centroids of the α-carbons of residues 210 and 213 in *Sa*FtsZ and the centroid of the terminal phosphate (γ-phosphate for GTP), then computing the mean distance between each α-carbon and the terminal phosphate. To correct for the virtual shift of the T7-nucleotide distance in GDP-bound subunits due to the loss of the γ-phosphate, a GTP molecule was aligned to GDP and then the T7-nucleotide distance was computed as above.

DiffNets analysis

Inputs for DiffNet training were prepared according to (Ward *et al.*, 2021) as follows: (1) NAMD trajectories were processed using VMD (Humphrey *et al.*, 1996) to extract the α-carbon trajectories; (2) trajectories were then converted from *dcd* format to *xtc* using the *mdconvert* command-line script from the MDTraj python package (McGibbon *et al.*, 2015); (3) trajectories were preprocessed using the whitening procedure detailed in the DiffNets package; (4) each DiffNet was trained using identical hyper-parameters (20 epochs, 50-fold dimensional reduction, 32 frame batch size, *nnutils.sae* architecture); (5) DiffNet clustering analysis was performed to identify key residue interactions, of which the top 50 were chosen for further analysis.

Structural variants of monomers in open and closed states were chosen based on sufficient sampling (at least 100 ns total trajectory length) and conformational stability. Open-state structural variants were selected from simulations of GDP-bound monomers with Mg^{2+} (Figure 1D), utilizing the first 30 ns of the first replicate (Figure 1D, light orange) and the first 70 ns of the second replicate (Figure 1D, orange). Closed-state structural variants were selected from 20 ns to 120 ns of the first replicate of the GDP-bound monomer simulation (Figure 1D, light blue).

Key residues were identified as those present in >5 of the top 50 residue–residue interactions obtained from the DiffNets *analyze* output. Additional prediction utilizing the trained DiffNet was performed with the *predict_new* function.

We thank members of the Huang lab for helpful discussions. This work was funded by a Stanford Interdisciplinary Graduate Fellowship (to B.D.K.), a James S. McDonnell Postdoctoral Fellowship (to H.S.), and NSF Award EF-2125383 (to K.C.H.). K.C.H. is a Chan Zuckerberg Biohub Investigator. The simulations were performed with computer time provided by the Extreme Science and Engineering Discovery Environment (XSEDE), which is supported by National Science Foundation Grant ACI-1548562, with allocation number TG-MCB110056 (to K.C.H.).

REFERENCES

Andreu JM, Schaffner-Barbero C, Huecas S, Alonso D, Lopez-Rodriguez ML, Ruiz-Avila LB, Nunez-Ramirez R, Llorca O, Martin-Galiano AJ (2010). The antibacterial cell division inhibitor PC190723 is an FtsZ polymer-stabilizing agent that induces filament assembly and condensation. J Biol Chem 285, 14239–14246.

Best RB, Zhu X, Shim J, Lopes PE, Mittal J, Feig M, Mackerell AD, Jr. (2012). Optimization of the additive CHARMM all-atom protein force field targeting improved sampling of the backbone phi, psi and side-chain chi(1) and chi(2) dihedral angles. J Chem Theory Comput 8, 3257–3273.

Bi EF, Lutkenhaus J (1991). FtsZ ring structure associated with division in *Escherichia coli*. Nature 354, 161–164.

Bisson-Filho AW, Hsu YP, Squyres GR, Kuru E, Wu F, Jukes C, Sun Y, Dekker C, Holden S, VanNieuwenhze MS, *et al.* (2017). Treadmilling by FtsZ filaments drives peptidoglycan synthesis and bacterial cell division. Science 355, 739–743.

Blaabjerg LM, Kassem MM, Good LL, Jonsson N, Cagiada M, Johansson KE, Boomsma W, Stein A, Lindorff-Larsen K (2023). Rapid protein stability prediction using deep learning representations. eLife 12, e82593.

Bordin N, Dallago C, Heinzinger M, Kim S, Littmann M, Rauer C, Steinegger M, Rost B, Orengo C (2023). Novel machine learning approaches revolutionize protein knowledge. Trends Biochem Sci 48, 345–359.

Cabeen MT, Jacobs-Wagner C (2010). The bacterial cytoskeleton. Annu Rev Genet 44, 365–392.

Chandra A, Tunnermann L, Lofstedt T, Gratz R (2023). Transformer-based deep learning for predicting protein properties in the life sciences. eLife 12, e82819.

Chen Y, Bjornson K, Redick SD, Erickson HP (2005). A rapid fluorescence assay for FtsZ assembly indicates cooperative assembly with a dimer nucleus. Biophys J 88, 505–514.

Colavin A, Hsin J, Huang KC (2014). Effects of polymerization and nucleotide identity on the conformational dynamics of the bacterial actin homolog MreB. Proc Natl Acad Sci USA 111, 3585–3590.

Conti J, Viola MG, Camberg JL (2018). FtsA reshapes membrane architecture and remodels the Z-ring in *Escherichia coli*. Mol Microbiol 107, 558–576.

Corbin LC, Erickson HP (2020). A Unified Model for Treadmilling and Nucleation of Single-Stranded FtsZ Protofilaments. Biophys J 119, 792–805.

Du S, Pichoff S, Kruse K, Lutkenhaus J (2018). FtsZ filaments have the opposite kinetic polarity of microtubules. Proc Natl Acad Sci USA 115, 10768–10773.

Fletcher DA, Mullins RD (2010). Cell mechanics and the cytoskeleton. Nature 463, 485–492.

Fujita J, Harada R, Maeda Y, Saito Y, Mizohata E, Inoue T, Shigeta Y, Matsumura H (2017). Identification of the key interactions in structural transition pathway of FtsZ from *Staphylococcus aureus*. J Struct Biol 198, 65–73.

Fujita J, Amesaka H, Yoshizawa T, Hibino K, Kamimura N, Kuroda N, Konishi T, Kato Y, Hara M, Inoue T (2023). Structures of a FtsZ single protofilament and a double-helical tube in complex with a monobody. Nat Commun 14, 4073.

Geggier S, Kotlyar A, Vologodskii A (2011). Temperature dependence of DNA persistence length. Nucleic Acids Res 39, 1419–1426.

Gittes F, Mickey B, Nettleton J, Howard J (1993). Flexural rigidity of microtubules and actin filaments measured from thermal fluctuations in shape. J Cell Biol 120, 923–934.

Guan F, Yu J, Yu J, Liu Y, Li Y, Feng XH, Huang KC, Chang Z, Ye S (2018). Lateral interactions between protofilaments of the bacterial tubulin homolog FtsZ are essential for cell division. eLife 7, e35578.

Hale CA, de Boer PA (1997). Direct binding of FtsZ to ZipA, an essential component of the septal ring structure that mediates cell division in *E. coli*. Cell 88, 175–185.

Haydon DJ, Stokes NR, Ure R, Galbraith G, Bennett JM, Brown DR, Baker PJ, Barynin VV, Rice DW, Sedelnikova SE, *et al*. (2008). An inhibitor of FtsZ with potent and selective anti-staphylococcal activity. Science 321, 1673–1675.

Hsin J, Gopinathan A, Huang KC (2012). Nucleotide-dependent conformations of FtsZ dimers and force generation observed through molecular dynamics simulations. Proc Natl Acad Sci USA 109, 9432–9437.

Huecas S, Llorca O, Boskovic J, Martin-Benito J, Valpuesta JM, Andreu JM (2008). Energetics and geometry of FtsZ polymers: nucleated self-assembly of single protofilaments. Biophys J 94, 1796–1806.

Humphrey W, Dalke A, Schulten K (1996). VMD: visual molecular dynamics. J Mol Graph 14: 33–38, 27–28.

Jorgensen JH, Johnson JE, Alexander GA, Paxson R, Alderson GL (1983). Comparison of automated and rapid manual methods for the same-day identification of Enterobacteriaceae. Am J Clin Pathol 79, 683–687.

Jumper J, Evans R, Pritzel A, Green T, Figurnov M, Ronneberger O, Tunyasuvunakool K, Bates R, Zidek A, Potapenko A, *et al*. (2021). Highly accurate protein structure prediction with AlphaFold. Nature 596, 583–589.

Knapp BD, Ward MD, Bowman GR, Shi H, Huang KC (2022). Multiple conserved states characterize the twist landscape of the bacterial actin homolog MreB. Comput Struct Biotechnol J 20, 5838–5846.

Li Y, Hsin J, Zhao L, Cheng Y, Shang W, Huang KC, Wang HW, Ye S (2013). FtsZ protofilaments use a hinge-opening mechanism for constrictive force generation. Science 341, 392–395.

Loose M, Mitchison TJ (2014). The bacterial cell division proteins FtsA and FtsZ self-organize into dynamic cytoskeletal patterns. Nat Cell Biol 16, 38–46.

Lowe J, Amos LA (1998). Crystal structure of the bacterial cell-division protein FtsZ. Nature 391, 203–206.

Lowe J, Amos LA (1999). Tubulin-like protofilaments in Ca^{2+}-induced FtsZ sheets. EMBO J 18, 2364–2371.

Lu C, Reedy M, Erickson HP (2000). Straight and curved conformations of FtsZ are regulated by GTP hydrolysis. J Bacteriol 182, 164–170.

Lv D, Li J, Ye S (2021). The Assembly Switch Mechanism of FtsZ Filament Revealed by All-Atom Molecular Dynamics Simulations and Coarse-Grained Models. Front Microbiol 12, 639883.

Mackerell AD, Jr., Feig M, Brooks CL, 3rd (2004). Extending the treatment of backbone energetics in protein force fields: limitations of gas-phase quantum mechanics in reproducing protein conformational distributions in molecular dynamics simulations. J Comput Chem 25, 1400–1415.

Matsui T, Han X, Yu J, Yao M, Tanaka I (2014). Structural change in FtsZ Induced by intermolecular interactions between bound GTP and the T7 loop. J Biol Chem 289, 3501–3509.

Matsui T, Yamane J, Mogi N, Yamaguchi H, Takemoto H, Yao M, Tanaka I (2012). Structural reorganization of the bacterial cell-division protein FtsZ from *Staphylococcus aureus*. Acta Crystallogr D Biol Crystallogr 68, 1175–1188.

McGibbon RT, Beauchamp KA, Harrigan MP, Klein C, Swails JM, Hernández CX, Schwantes CR, Wang L-P, Lane TJ, Pande VS (2015). MDTraj: a modern open library for the analysis of molecular dynamics trajectories. Biophys J 109, 1528–1532.

Miguel A, Hsin J, Liu T, Tang G, Altman RB, Huang KC (2015). Variations in the binding pocket of an inhibitor of the bacterial division protein FtsZ across genotypes and species. PLoS Comput Biol 11, e1004117.

Miraldi ER, Thomas PJ, Romberg L (2008). Allosteric models for cooperative polymerization of linear polymers. Biophys J 95, 2470–2486.

Mukherjee A, Lutkenhaus J (1999). Analysis of FtsZ assembly by light scattering and determination of the role of divalent metal cations. J Bacteriol 181, 823–832.

Oliva MA, Cordell SC, Lowe J (2004). Structural insights into FtsZ protofilament formation. Nat Struct Mol Biol 11, 1243–1250.

Pereira AR, Hsin J, Krol E, Tavares AC, Flores P, Hoiczyk E, Ng N, Dajkovic A, Brun YV, VanNieuwenhze MS, *et al.* (2016). FtsZ-Dependent Elongation of a Coccoid Bacterium. mBio 7, e00908.

Ramirez-Aportela E, Lopez-Blanco JR, Andreu JM, Chacon P (2014). Understanding nucleotide-regulated FtsZ filament dynamics and the monomer assembly switch with large-scale atomistic simulations. Biophys J 107, 2164–2176.

Ramirez-Diaz DA, Merino-Salomon A, Meyer F, Heymann M, Rivas G, Bramkamp M, Schwille P (2021). FtsZ induces membrane deformations via torsional stress upon GTP hydrolysis. Nat Commun 12, 3310.

Rivas G, Lopez A, Mingorance J, Ferrandiz MJ, Zorrilla S, Minton AP, Vicente M, Andreu JM (2000). Magnesium-induced linear self-association of the FtsZ bacterial cell division protein monomer. The primary steps for FtsZ assembly. J Biol Chem 275, 11740–11749.

Ruiz FM, Huecas S, Santos-Aledo A, Prim EA, Andreu JM, Fernandez-Tornero C (2022). FtsZ filament structures in different nucleotide states reveal the mechanism of assembly dynamics. PLoS Biol 20, e3001497.

Scheffers DJ, den Blaauwen T, Driessen AJ (2000). Non-hydrolysable GTP-gamma-S stabilizes the FtsZ polymer in a GDP-bound state. Mol Microbiol 35, 1211–1219.

Schumacher MA, Ohashi T, Corbin L, Erickson HP (2020). High-resolution crystal structures of *Escherichia coli* FtsZ bound to GDP and GTP. Acta Crystallogr F Struct Biol Commun 76, 94–102.

Shaevitz JW, Gitai Z (2010). The structure and function of bacterial actin homologs. Cold Spring Harb Perspect Biol 2, a000364.

Shi H, Quint DA, Grason GM, Gopinathan A, Huang KC (2020). Chiral twisting in a bacterial cytoskeletal polymer affects filament size and orientation. Nat Commun 11, 1408.

Tuckerman M, Berne BJ, Martyna GJ (1992). Reversible multiple time scale molecular dynamics. J Chem Phys 97, 1990–2001.

Turner DJ, Portman I, Dafforn TR, Rodger A, Roper DI, Smith CJ, Turner MS (2012). The mechanics of FtsZ fibers. Biophys J 102, 731–738.

Typas A, Banzhaf M, Gross CA, Vollmer W (2011). From the regulation of peptidoglycan synthesis to bacterial growth and morphology. Nat Rev Microbiol 10, 123–136.

Wagstaff JM, Tsim M, Oliva MA, Garcia-Sanchez A, Kureisaite-Ciziene D, Andreu JM, Lowe J (2017). A Polymerization-Associated Structural Switch in FtsZ That Enables Treadmilling of Model Filaments. mBio 8, e00254.

Ward MD, Zimmerman MI, Meller A, Chung M, Swamidass SJ, Bowman GR (2021). Deep learning the structural determinants of protein biochemical properties by comparing structural ensembles with DiffNets. Nat Commun 12, 3023.

Yang X, Lyu Z, Miguel A, McQuillen R, Huang KC, Xiao J (2017). GTPase activity-coupled treadmilling of the bacterial tubulin FtsZ organizes septal cell wall synthesis. Science 355, 744–747.

Yoshizawa T, Fujita J, Terakado H, Ozawa M, Kuroda N, Tanaka SI, Uehara R, Matsumura H (2020). Crystal structures of the cell-division protein FtsZ from *Klebsiella pneumoniae* and *Escherichia coli*. Acta Crystallogr F Struct Biol Commun 76, 86–93.